Received: 30 January 2018 | Accepted: 4 April 2018

DOI: 10.1002/mrc.4742

RESEARCH ARTICLE

WILEY

Imaging of copper oxygenation reactions in a bubble flow

Stefan Benders[1] | Florian Strassl[2] | Bastian Fenger[1] | Bernhard Blümich[1] | Sonja Herres-Pawlis[2] | Markus Küppers[1]

[1]Institut für Technische und Makromolekulare Chemie, RWTH Aachen University, Aachen 52074, Germany

[2]Institut für Anorganische Chemie, RWTH Aachen University, Aachen 52074, Germany

Correspondence
Stefan Benders, RWTH Aachen University, Institut für Technische und Makromolekulare Chemie, Aachen 52074, Germany.
Email: Stefan.Benders@rwth-aachen.de

Funding information
Deutsche Forschungsgemeinschaft (DFG), Grant/Award Number: HE5480/10-1

Reactions of gases with liquids play a crucial role in the production of many bulk chemicals. Often, the gas is bubbled into the chosen reactor. Most of the processes at the gas–liquid interface of the bubbles and in their tails are not fully understood and warrant further investigation. For this purpose, NMR imaging or Magnetic Resonance Imaging has been applied to visualize some of the processes in the bubble tail. To generate sufficient contrast, a magnetogenic gas–liquid reaction associated with a change of magnetic state, from diamagnetic to paramagnetic, was employed. In this work, a copper(I)-based compound was oxidized to copper(II) to exploit relaxation contrast. To match the speed of the rising bubbles to the acquisition time of the spin-echo imaging sequence, polyethylene glycol was added to increase the viscosity of the reacting solution. Images of the oxygen ingress into a static solution as well as of oxygen bubbles rising in the solution are presented. In both cases, changes in magnetism were observed, which reported the hydrodynamic processes.

KEYWORDS
bubble flow, chemical engineering, contrast agents, magnetic resonance imaging, ^{1}H

1 | INTRODUCTION

Bubble-column reactors play a crucial role in large-scale industrial processes, such as the Wacker–Hoechst oxidation.[1] Although a considerable amount of research has been invested to understand single bubble phenomena,[2,3] the interactions of multiple bubbles,[4,5] and even whole bubble reactors,[6,7] there is growing interest in understanding the chemical processes in the bubble tail. These processes can be spatially resolved with Magnetic Resonance Imaging (MRI).[8–13] It has been applied in chemical engineering, for example, to investigate fouling of membranes,[14,15] droplet dynamics,[16,17] fluidized beds,[18,19] rock cores,[20,21] and porous filters.[22] So far, studies on droplet dynamics and fluidized beds mostly focused on visualizing the bubble path, measuring the bubble-rise velocity and investigating internal fluid dynamics. This study focuses on the bubble tail and the reactions occurring there. It is difficult to visualize processes in this region, since these processes are fast and hard to detect with common MRI contrast such as spin density, T_1 or T_2. To visualize such processes, classical chemical shift imaging (CSI)[23] could be employed, but it is not pursued here because the acquisition time is too long. Therefore, one of such a process is visualized with a contrast agent specially designed for oxygen–liquid reactions. This approach relates to magnetogenics, where chemical probes react to the chemical environment of molecules and change the relaxation parameters. They are most valuable in medicine.[24–26] Moreover there are applications to visualizing chemical waves.[27] Here, an application to chemical engineering is presented.

In these experiments, oxidation of copper(I) to copper(II) is responsible for the contrast. Many copper N-donor complexes activate dioxygen and a multitude of Cu-dioxygen species has been established in the last

decades.[29,30] These studies are bioinspired since nature also uses dicopper sites in hemocyanin to transport dioxygen in arthropods and molluscs and in tyrosinase to activate it for phenol oxygenation in browning processes in mammals, birds but also vegetables and fruits.[29–31] Copper(I) reduces the molecular oxygen to a peroxide moiety under formation of a side-on-peroxo copper(II) complex but with many ligand systems, the oxygen reduction proceeds to the oxido state realized in bis(μ-oxo) dicopper(III) complexes.[29,30] Using guanidine ligands, bis(μ-oxo) dicopper(III) complexes can be selectively addressed.[32,33] These copper(III) species decay to paramagnetic copper(II) species later, and this effect can be used for monitoring by fluorescence spectroscopy.[34] With regard to NMR, we try to use the difference of relaxation times between the diamagnetic copper(I) and the paramagnetic copper(II) for imaging purposes.

2 | EXPERIMENTAL

2.1 | Sample preparation

The copper complex (Cu bis(tetramethylguanidino) propylene, [Cu(btmgp)I], Figure 1) was synthesized as described by Pohl et al.[35] and then stored under inert gas atmosphere due to its high reactivity with oxygen. For the bubble-rise experiments, a solution of polyethylene glycol (PEG, $M_n = 4 \times 10^6$ g/mol) in acetonitrile with a viscosity of roughly 800 mPas was prepared and degassed, whereas for gas-ingress visualization, pure acetonitrile was utilized. Afterwards, 20 mg (100 mg for the ingress experiment) of [Cu(btmgp)I] was dissolved in this solution and transferred into a 20-mm-diameter reactor made from PEEK. The reactor provides the ability to fill in samples through a septum, while inert gas is flowing through the reactor to avoid oxygen contamination. The flow is realized with two gas inlet/outlet ports (Figure 2), which were later used for oxygen supply. A tube was glued to these ports from the inside for the bubble rise experiments to guide the gas to the bottom of the reactor.

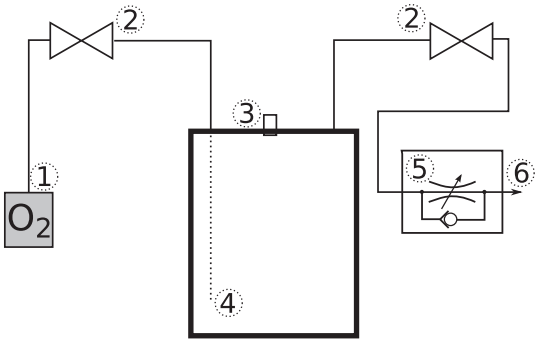

FIGURE 2 Sketch of the reactor used. 1: (99%) Oxygen bottle with valves; 2: shut-off valve; 3: septum for fluid handling; 4: tube glued to the bottom (optional); 5: throttle check valve; 6: gas outlet

2.2 | NMR experiments

The gas ingress was visualized in experiments with a Bruker Avance 500 spectrometer, whereas the bubbles were visualized in experiments with a Bruker Avance 700 spectrometer. In both cases, a Micro2.5 gradient system (max. gradient strength 1.5 T/m) with a 20-mm Birdcage resonator and the Multi-Slice-Multi-Echo (MSME) pulse sequence provided by the Paravision 4.0/5.1 software package were used. Additionally, in the ingress experiment, a preparation pulse (180° , preparation time: 100 ms) was employed to enhance contrast. General parameters: 90°/180°-pulse: sinc3 1 ms/0.75 ms. *Ingress*

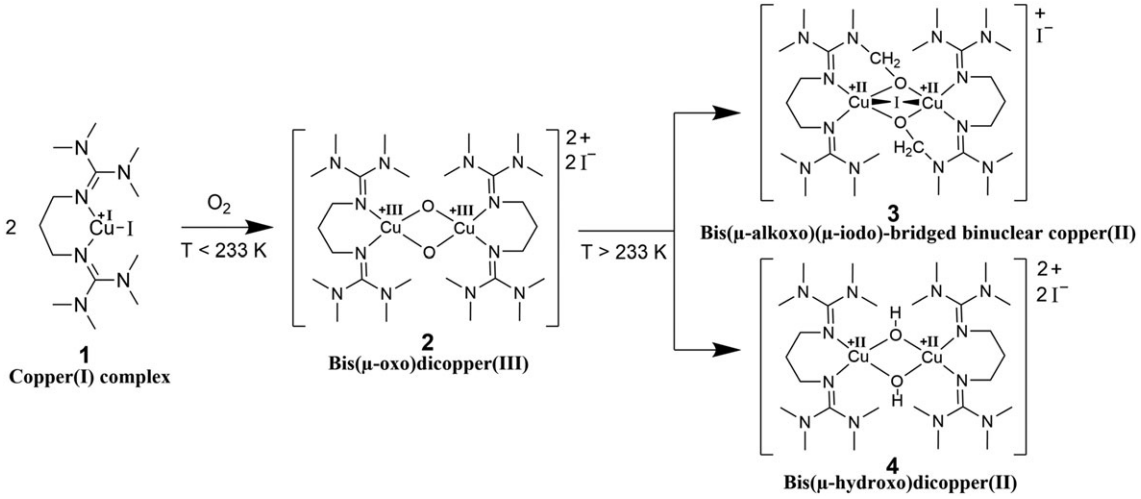

FIGURE 1 Reaction system. The copper(I) complex reacts with oxygen to the bis-(μ-oxo)-dcopper(III) species. At temperatures above −40 ° C, the Cu(III) species rapidly decays to the bis-μ-hydroxo Cu(II) and the bis-(μ-alkoxo)(μ-iodo) Cu(II) bridged binuclear species[28]

experiment with field-of-view: $39.4 \times 22\,mm^2$, spatial resolution: $0.08 \times 0.18\,mm^2$, slice thickness: 4 mm, preparation time: 100 ms, repetition time: 113 ms, echo time: 7.44 ms. *Bubble experiment* with field-of-view: $50 \times 25\,mm^2$, spatial resolution: $0.39 \times 0.39\,mm^2$, slice thickness: 8.35 mm, repetition time: 50 ms, echo time: 3.24 ms.

3 | RESULTS

3.1 | Copper complex contrast

[Cu(btmgp)I] consists of a copper(I) metal center, which is coordinated by a bis(tetramethylguanidino)propylene (btmgp) ligand. In contact with oxygen, two units first react to a copper(III) bis(μ-oxo) complex, which rapidly decays at temperatures above −40 °C to a Cu(II) complex. The reaction speed can be adjusted by choice of ligand and temperature. In this case, with the btmgp ligand at room temperature, the typical time of reaction is 4 s.[36] In NMR, the transition of copper(I) to copper(II) is clearly visible by a change of relaxation parameters. Copper(II) is paramagnetic and, therefore, shortens the relaxation times T_2 and T_1. In this study, T_1 was chosen as the contrast parameter and is accessed through saturation and/or inversion preparation modules.

3.2 | Gas ingress visualization

In an effort to visualize gas–liquid reactions by MRI utilizing [Cu(btmgp)I], the gas ingress of oxygen into a solution of [Cu(btmgp)I] was investigated. For this purpose, the oxygen flow was channeled along the surface of the solution. An image of the solution was acquired every 14.45 s with a 180 ° preparation pulse 100 ms prior to acquisition and a repetition time of 109 ms. These parameters lead to a strong signal for the product species (Cu(II)) in the images (Figure 3). Vortice-shaped profiles can be observed after a short time followed by a full transition of the copper(I) complex in solution to copper(II) within 30 min.

3.3 | Reactions in the bubble tail

After the first studies proved the possibility to visualize gas ingress into the solution, more complex gas–liquid interactions were investigated. For this purpose, a tube was glued to the gas inlet of the reactor and a very small oxygen flow was bubbled through the viscous solution while imaging. The parameters were changed (no preparation pulse, 50 ms repetition time) to increase the imaging speed. In Figure 4 rising bubbles and their tails can be observed. In both measurements, the rise of the bubble can be clearly observed, and a high NMR signal caused by generation of the copper(II) species indicates the reactions occurring in the bubble tail. Furthermore, the bubble size decreases on its rise due to the consumption of oxygen in the reaction. After a few bubbles, the bubbles can hardly be seen due to masking of strong signal originating from the copper(II) species. Assuming that T_2 effects of varying copper(II) concentration do not play a significant role in contrast generation, the reaction progress can be mapped. The signal equation can be simplified to:

$$I(c(Cu^{2+})) = I_0 \cdot \exp(-r_2 \cdot t_{Echo}) \cdot (1 - \exp(-r_1 \cdot t_{rep})) \quad (1)$$

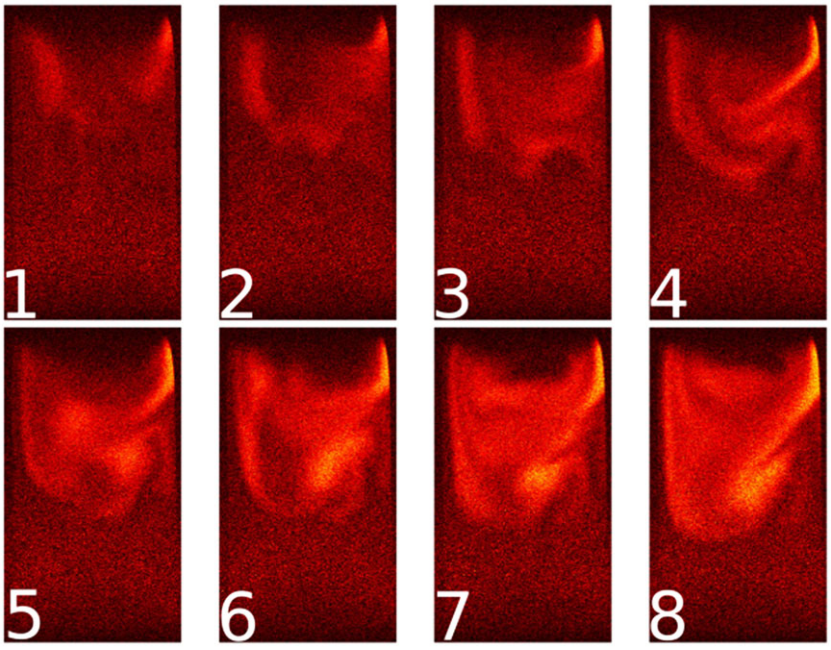

FIGURE 3 Visualization of gas ingress to a acetonitrile solution of [Cu(btmgp)I] with an image separation of 14.45 s

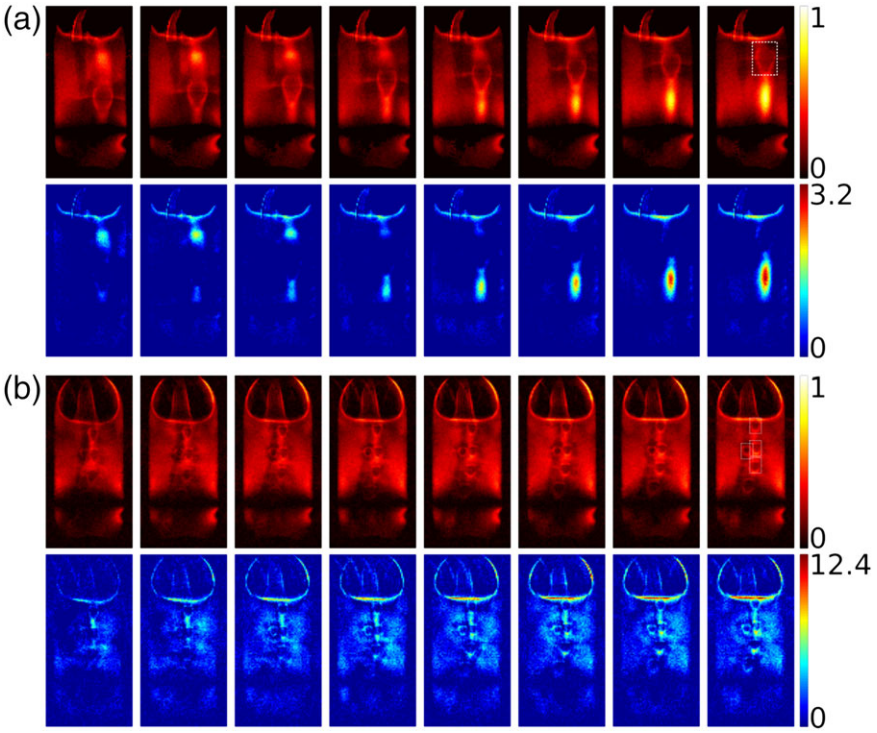

FIGURE 4 Monitoring the rise of one bubble and the reaction in its tail. One image was acquired every 3.2 s. In the top row, the raw spin density images are depicted whereas in the bottom row the calculated relative concentration maps are depicted. The invisible area on the bottom in the top row is an artifact from the birdcage resonator. The oxygen flow rate in (b) was decreased compared to (a)

with the image amplitude I_0, the transverse relaxation rate r_2, the echo time t_{Echo}, the longitudinal relaxation rate r_1 and the repetition time t_{rep}. For small concentrations, the relaxation rate r_1 is proportional to the concentration, $r_1 = k \cdot c(\text{Cu}^{2+}) + r_{1,0}$, so that

$$\begin{aligned} I(c(\text{Cu}^{2+})) = I_0 \cdot \exp(-r_2 \cdot t_{\text{Echo}}) \\ \cdot (1 - \exp(-k \cdot c(\text{Cu}^{2+}) \\ \cdot t_{\text{rep}} - r_{1,0} \cdot t_{\text{rep}})) \end{aligned} \quad (2)$$

Subtracting the initial signal in $I_{\text{r}} = I(c(\text{Cu}^{2+})) - I(c(\text{Cu}^{2+}) = 0)$ yields:

$$\begin{aligned} I_{\text{r}} = I_0 \cdot \exp(-r_2 \cdot t_{\text{Echo}}) \\ \cdot \exp(-r_{1,0} \cdot t_{\text{rep}}) \\ \cdot (1 - \exp(-k \cdot c(\text{Cu}^{2+}) \cdot t_{\text{rep}})) \end{aligned} \quad (3)$$

Expanding the expression $1 - \exp(-x)$ into a series and neglecting terms higher than first order since the concentrations are small leads to

$$I_{\text{r}} = I_0 \cdot \exp(-r_2 \cdot t_{\text{Echo}}) \cdot \exp(-r_{1,0} \cdot t_{\text{rep}}) \cdot k \cdot c(\text{Cu}^{2+}) \cdot t_{\text{rep}}. \quad (4)$$

Therefore, the resultant intensity is proportional to the concentration. Unfortunately, not all parameters are known as they depend on many influences such as gas content and composition of the solution, remaining water content of the solvent, and the state of reaction of the solid complex. Therefore, the concentration can be mapped only in relative terms shown in Figure 4, whereby the oxidation of copper(I) can be observed mainly in the bubble tail.

The bubble size and rise velocity in a bubble-column reactor are two of the most important quantities. The velocity in the experiments presented here can be estimated by following the characteristic spin density drop in 1D-projections on the bubble path throughout the images. In doing so, a bubble-size of approximately 2 mm and a velocity of 0.50 mm/s for the reaction in Figure 4a and bubble sizes ranging from 0.8 to 0.9 mm and velocities ranging from 0.14 to 0.25 mm/s for Figure 4b can be estimated.

4 | SUMMARY AND CONCLUSIONS

The use of contrast agents such as diamagnetic copper complexes enables MRI visualization of chemical processes due to relaxation contrast. The copper complex utilized is a model system, which is simple to use and generates good contrast by rapid change of the oxidation state upon contact with oxygen. Gas–liquid reactions such as the one presented here are an important fraction of the chemical processes, which can be visualized by MRI. Magnetogenic agents can help to understand processes in the gas–liquid interface without the need of time-consuming complex pulse sequences such as chemical-shift-imaging.

Processes in chemical engineering such as filtration, mixing, gas enrichment are expected to benefit from such a research methodology.

ACKNOWLEDGEMENTS

The authors thank Ralf Theelen for construction of the PEEK reactor and Sören Lehmkuhl for helpful advice concerning the sample preparation. Sonja Herres-Pawlis and Florian Strassl gratefully acknowledge funding by the Deutsche Forschungsgemeinschaft (DFG) in the frame of the Priority Program 1740 'The Influence of Local Transport Processes on Chemical Reactions in Bubble Flows' (grant number HE5480/10-1).

ORCID

Stefan Benders http://orcid.org/0000-0002-9823-1928
Florian Strassl http://orcid.org/0000-0002-9656-2838
Bernhard Blümich http://orcid.org/0000-0002-1152-4438
Sonja Herres-Pawlis http://orcid.org/0000-0002-4354-4353
Markus Küppers http://orcid.org/0000-0002-0751-8799

REFERENCES

[1] J. Smidt, W. Hafner, R. Jira, J. Sedlmeier, R. Sieber, R. Rüttinger, H. Kojer. *Angew. Chem.* **1959**, *71*(5), 176.

[2] A. A. Kulkarni, J. B. Joshi. *Ind. Eng. Chem. Res.* **2005**, *44*(16), 5873, https://doi.org/10.1021/ie049131p.

[3] M. Wu, M. Gharib. *Phys. Fluids* **2002**, *14*(7), L49, https://doi.org/10.1063/1.1485767.

[4] J. Timmermann, M. Hoffmann, M. Schlüter. *Chem. Eng. Technol.* **2016**, *39*(10), 1955.

[5] T. Sanada, A. Sato, M. Shirota, M. Watanabe. *Chem. Eng. Sci.* **2009**, *64*(11), 2659.

[6] M. Bothe, M. A. Christlieb, M. Hoffmann, O. Tedjasukmana, F. Michaux, P. Rollbusch, M. Becker, M. Schlüter. *Can. J. Chem. Eng.* **2017**, *95*(5), 902.

[7] Y. T. Shah, B. G. Kelkar, S. P. Godbole, W. D. Deckwer. *AIChE J.* **1982**, *28*(3), 353, https://doi.org/10.1002/aic.690280302.

[8] B. Blümich, *NMR imaging of materials*, *57*, OUP, Oxford **2000**.

[9] P. T. Callaghan, *Principles of nuclear magnetic resonance microscopy*, Oxford Science Publications, Clarendon Press, Oxford **1993**.

[10] S. Stapf, S. I. Han, *Nmr imaging in chemical engineering*, Wiley-VCH, Weinheim **2006**.

[11] B. Blümich, Winfried Kuhn, *Magnetic resonance microscopy: Methods and applications in materials science, agriculture and biomedicine*, Wiley-VCH, Weinheim **1992**.

[12] P. Blümler, B. Blümich, R. E. Botto, E. Fukushima, *Spatially resolved magnetic resonance*, Wiley-VCH, Weinheim **1998**.

[13] S. L. Codd, J. D. Seymour, *Magnet resonance microscopy*, Wiley-VCH, Weinheim **2009**.

[14] P. Z. Çulfaz, S. Buetehorn, L. Utiu, M. Küppers, B. Blümich, T. Melin, M. Wessling, R. G. H. Lammertink. *Langmuir* **2011**, *27*(5), 1643.

[15] F. Arndt, U. Roth, H. Nirschl, S. Schütz, G. Guthausen. *AIChE J.* **2016**, *62*(7), 2459.

[16] A. Amar, B. Blümich, F. Casanova. *Chemphyschem: Eur. J. Chem. Phys. Phys. Chem.* **2010**, *11*(12), 2630.

[17] S. I. Han, S. Stapf, B. Blümich. *Phys. Rev. Lett.* **2001**, *87*(14), 144501.

[18] H. T. Fabich, A. J. Sederman, D. J. Holland. *J. Magn. Reson.* **2016**, *273*, 113.

[19] S. Harms, S. Stapf, B. Blümich. *J. Magn. Reson.* **2006**, *178*(2), 308.

[20] F. Marica, Q. Chen, A. Hamilton, C. Hall, T. Al, B. J. Balcom. *J. Magn. Reson.* **2006**, *178*(1), 136.

[21] A. A. Colbourne, A. J. Sederman, M. D. Mantle, L. F. Gladden. *J. Magn. Reson.* **2016**, *272*, 68.

[22] L. Huang, G. Mikolajczyk, E. Küstermann, M. Wilhelm, S. Odenbach, W. Dreher. *J. Magn. Reson.* **2017**, *276*, 103.

[23] P. C. Lauterbur, D. M. Kramer, W. V. House, C. N. Chen. *J. Am. Chem. Soc.* **1975**, *97*(23), 6866.

[24] E. S. O'Neill, J. L. Kolanowski, G. H. Yin, K. M. Broadhouse, S. M. Grieve, A. K. Renfrew, P. D. Bonnitcha, E. J. New. *RSC Adv.* **2016**, *6*(36), 30021.

[25] J. Hasserodt. *New J. Chem.* **2012**, *36*(9), 1707.

[26] C. Gondrand, F. Touti, E. Godart, Y. Berezhanskyy, E. Jeanneau, P. Maurin, J. Hasserodt. *Eur. J. Inorg. Chem.* **2015**, *2015*(8), 1376.

[27] A. Tzalmona, R. L. Armstrong, M. Menzinger, A. Cross, C. Lemaire. *Chem. Phys. Lett.* **1990**, *174*(2), 199.

[28] S. Herres, A. J. Heuwing, U. Flörke, J. Schneider, G. Henkel. *Inorg. Chim. Acta* **2005**, *358*(4), 1089.

[29] E. I. Solomon, D. E. Heppner, E. M. Johnston, J. W. Ginsbach, J. Cirera, M. Qayyum, M. T. Kieber-Emmons, C. H. Kjaergaard, R. G. Hadt, L. Tian. *Chem. Rev.* **2014**, *114*(7), 3659, https://doi.org/10.1021/cr400327t. PMID: 24588098.

[30] J. N. Hamann, B. Herzigkeit, R. Jurgeleit, F. Tuczek. *Coord. Chem. Rev.* **2017**, *334*, 54. Small Molecule Activation.

[31] J. L. Muñoz-Muñoz, J. Berna, M. del Mar García-Molina, F. Garcia-Molina, P. A. Garcia-Ruiz, R. Varon, J. N. Rodriguez-Lopez, F. Garcia-Canovas. *Biochem. Biophys. Res. Commun.* **2012**, *424*(2), 228.

[32] S. Herres-Pawlis, P. Verma, R. Haase, P. Kang, C. T. Lyons, E. C. Wasinger, U. Flörke, G. Henkel, T. D. P. Stack. *J. Am. Chem. Soc.* **2009**, *131*(3), 1154, https://doi.org/10.1021/ja807809x. PMID: 19119846.

[33] S. Herres-Pawlis, R. Haase, P. Verma, A. Hoffmann, P. Kang, T. D. P. Stack. *Eur. J. Inorg. Chem.* **2015**, *2015*(32), 5426.

[34] S. Herres-Pawlis, G. Berth, V. Wiedemeier, L. Schmidt, A. Zrenner, H. J. Warnecke. *J. Lumin.* **2010**, *130*(10), 1958.

[35] T. I. S. Pohl, M. Harmjanz, J. Schneider, W. Saak, G. Henkel. *J. Chem. Soc. Dalton Trans.* **2000**, 3473, https://doi.org/10.1039/B002554M.

[36] D. Schurr, F. Strassl, P. Liebhäuser, G. Rinke, R. Dittmeyer, S. Herres-Pawlis. *React. Chem. Eng.* **2016**, *1*(5), 485.

How to cite this article: Benders S, Strassl F, Fenger B, Blümich B, Herres-Pawlis S, Küppers M. Imaging of copper oxygenation reactions in a bubble flow. *Magn Reson Chem*. 2018;1–5. https://doi.org/10.1002/mrc.4742